Analysis of Various Drained and Undrained Instability Modes in Medium Dense Sand Subjected to Biaxial Loading Conditions

Mousumi Mukherjee, Ph.D.[1]; Anurag Gupta, Ph.D.[2]; and Amit Prashant, Ph.D.[3]

[1]Former Research Scholar, Dept. of Civil Engineering, Indian Institute of Technology Kanpur, India. E-mail: mousumi.ju06@gmail.com
[2]Associate Professor, Dept. of Mechanical Engineering, Indian Institute of Technology Kanpur, India. E-mail: ag@iitk.ac.in
[3]Professor, Dept. of Civil Engineering, Indian Institute of Technology Gandhinagar, India. E-mail: ap@iitgn.ac.in

Abstract

The present study theoretically explores instability behavior of medium dense sand under both drained and undrained biaxial test. The instability analysis has been posed as a plane strain bifurcation problem within a large deformation framework. A generalized pressure-dependent 3D constitutive model has been employed to simulate the drained and undrained biaxial tests on a medium dense sand sample assuming two types of lateral boundaries, namely rigid and flexible. The lateral boundary condition can influence significantly the onset of undrained soild-fluid instability and drained diffused intabilities. Localization gets delayed with increasing lateral confinement for both drained and undrained cases. Elastic parameters have strong impact on the instability onset.

INTRODUCTION

Plastic instabilities of various form, e.g., volume instability, bulging, buckling or shear bands, are often encountered during laboratory testing of soil specimen. Such instabilities induce nonuniform deformation field in the specimen and act as a precursor to failure. Emergence of these instability modes depends on the material properties, type of loading, and boundary conditions. Shear bands are the most commonly observed instability modes in case of biaxial experiments on saturated sand (Desrues et al 1985; Han and Vardoulakis 1991; Finno et al. 1997). The level of confinement in such tests can significantly influence the onset of localization and shear band angle (Desrues and Hammad 1989; Han and Drescher 1993). Desrues and Hammad (1989) observed that localization in biaxial test gets significantly delayed with increase in confining pressure or decrease in density. Furthermore, antisymmetric diffused modes (i.e., buckling) were also encountered in the experiments on loose sands at high confining pressure. In addition to localized instabilities, liquefaction type solid-fluid instability modes are also frequently noticed in undrained tests of loose/medium dense sand (Han and Vardoulakis 1991).

Hill and Hutchinson (1975) proposed a bifurcation based analytical framework for analysing various non-unique deformation modes that can emerge from a uniform shear-free stress-strain field during tensile testing of incompressible solids under plane strain condition. Compressibility, non-associativity, pressure-sensitivity and lateral confinement was further incorporated in the formulation by other researchers (Needleman 1979, Vardoulakis 1981). Vardoulakis (1985) extended the plane-strain bifurcation analysis to water saturated

compressible media by taking into account the diffusion process. Bardet (1991), Bardet and Shiv (1995) presented a more general analytical approach to address plane strain bifurcation of elasto-plastic solids. However, simple plane-strain type Mohr-Coulomb model used in these analyses cannot explain the variations observed in the instability modes during experiments and a better representation of stress-strain relation is required for predicting instability modes at different stress states and drainage conditions. A generalized pressure dependent 3D constitutive model with hardening is expected to predict instability behavior more closely to the experimental observations and will also provide insights for different instability modes. Previously, Gajo et al. (2004) employed a 3D constitutive model and small deformation formulation to predict localization onset and post localization behavior of sand in drained biaxial test at varying initial density and confining pressure. More recently, Mukherjee et al. (2016a, 2016b) employed a large deformation framework along with a 3D material model to explore different undrained and drained instabilities that can emerge during biaxial test of sand subjected to various material state and boundary conditions. Following a similar approach, the present study attempts to examine theoretically the instability behavior of medium dense sand under both drained and undrained biaxial test.

The instability analysis has been posed as a plane strain bifurcation problem within a large deformation framework. A generalized pressure-dependent 3D constitutive model has been employed which accounts for the intermediate principal stress evolution under plane strain condition. Drained and undrained biaxial test simulations have been performed for a medium dense sand sample assuming both rigid and flexible lateral boundaries. Liquefaction type solid-fluid undrained instabilities, localization, antisymmetric and symmetric diffused drained modes have been explored here at different confining pressure and boundary condition.

MATERIAL MODEL

A generalized 3D non-associative constitutive model proposed by Wood et al. (1994) has been employed in this study. The model is based on critical state concept and includes both shear and volumetric hardening which enables to incorporate the effect of both density and confining pressure. The material behavior is characterized by the following incremental elasto-plastic stress-strain relation

$$\overset{\nabla}{\tau}{}'_{ij} = C_{ijkl} D_{kl} , \tag{1}$$

where $\overset{\nabla}{\boldsymbol{\tau}}{}'$ is the Jaumann rate of effective Kirchhoff stress, **D** is the rate of deformation tensor and C_{ijkl} is a fourth order tensor representing the elasto-plastic tangent stiffness of the material. The elastic response of the material is assumed to be linear and the plastic response is governed by the yield surface (f) & plastic potentials (g) with the following form

$$f(\tau', \varepsilon_q^p, \varepsilon_v^p) = \sqrt{3J_2} + \eta_y \frac{I_1'}{3} = 0 \ , \ \ g(\tau') = \sqrt{3J_2} + M_c \frac{I_1'}{3} \ln \frac{3P_r'}{I_1'} = 0 \ . \tag{2}$$

In the above expressions, ε_q^p and ε_v^p are the shear and volumetric components of logarithmic plastic strain tensor, I_1' is first invariant of effective Kirchhoff stress tensor, J_2 is second invariant of deviatoric Kirchhoff stress tensor, P_r' is the intercept of plastic potential on the $I_1'/3$

axis, η_y is shear stress ratio ($-3\sqrt{3J_2}/I_1^{'}$) which acts as a state variable and controls the hardening/softening response. The evolution of η_y is related to ε_q^p by the following function

$$\eta_y/\eta_p = \varepsilon_q^p/\left(a+\varepsilon_q^p\right), \tag{3}$$

where η_p is peak shear stress ratio defined as a function of another state variable ψ which includes information of specific volume v_e and mean stress

$$\eta_p = M_c - \kappa\psi = M_c - \kappa\left[v_e - \Gamma + \Lambda_c \ln\left(-I_1^{'}/3\right)\right]. \tag{4}$$

Here a, κ, M_c, Λ_c and Γ are the model parameters and their details are given in Table 1.

Table 1: Material constants considered in the analysis (Gajo et al., 2004)

Parameter	Description	Value
ν	Poisson's ratio	0.1
μ	Shear modulus	$G_0/3$ **
a	Parameter controlling hyperbolic stiffness relationship	0.0016
κ	Relation between changes in ψ and η_p	2
M_C	Slope of critical state line in $\sqrt{3J_2}$ - $\left(-I_1^{'}/3\right)$ plane	1.2
Λ_C	Slope of critical state line in v_e - $\ln(-I_1^{'}/3)$ plane	0.03
Γ	Intercept for critical state line in v_e - $\ln(-I_1^{'}/3)$ plane at 1 kPa effective mean pressure	1.969

** G_0 is the small strain shear modulus which is function of v_e and $I_1^{'}/3$ expressed in kPa (Hardin and Black, 1966), $G_0 = 3230\left\{(3.97-v_e)^2/v_e\right\}\sqrt{-I_1^{'}/3}$.

THEORETICAL FORMULATION

Governing equations: The mathematical framework for plane strain bifurcation analysis of a saturated soil sample under drained and undrained condition has been presented here briefly and the details can be found elsewhere (Vardoulakis 1981, 1985; Bardet 1991; Bardet and Shiv 1995; Mukherjee et al, 2016a, 2016b). If the deformed configuration has been considered as the present configuration, then in absence of body force and shear stress ($\sigma_{12} = \sigma_{21} = 0$) the stress rate equilibrium equations under undrained biaxial condition is given as

$$\overset{\nabla}{\sigma}{}^{'}_{11,1} + \overset{\nabla}{\sigma}{}^{'}_{21,1} - \left(\sigma^{'}_{11} - \sigma^{'}_{22}\right)W_{12,2} = \dot{p}_{,1}\ , \quad \overset{\nabla}{\sigma}{}^{'}_{12,1} + \overset{\nabla}{\sigma}{}^{'}_{22,2} - \left(\sigma^{'}_{11} - \sigma^{'}_{22}\right)W_{12,2} = \dot{p}_{,2}\ , \tag{5}$$

where, $\boldsymbol{\sigma}^{'}$ is the effective Cauchy stress, **W** is the spin tensor and p is the pore pressure. Notationally, dilation and stresses in tension are considered to be positive in this analysis. For an incompressible pore fluid, the continuity equation is given by

$$p_{,11} + p_{,22} = b\left(v_{1,1} + v_{2,2}\right), \tag{6}$$

where, $\boldsymbol{v}$ is velocity, $b = \gamma_w/\kappa_h$, γ_w and κ_h are the fluid unit weight and hydraulic permeability, respectively. Eq. 5 also represents the rate equations for drained condition when $p = 0$.

Boundary condition: The perturbed velocity fields assumed for bifurcation analysis should satisfy the boundary conditions depicted in Figure 1. For undrained case, fluid flow is not allowed across the boundaries. In case of rigid lateral boundary, the sample is subjected to constant velocities in both x_1 and x_2 direction at the boundaries $x_1 = \pm L_1$ and $x_2 = \pm L_2$, respectively. For flexible lateral boundary case, the top and bottom boundary ($x_2 = \pm L_2$) of the soil sample are given constant velocity in x_2 direction and the lateral surfaces are subjected to constant σ_{11}. The stress boundary conditions are imposed in terms of nominal stress rate ($\dot{\boldsymbol{S}}$). The stress-strain field initially remains homogeneous, with continued loading, an inhomogeneous stress-strain rate field may emerge due to bifurcation while satisfying the same equilibrium and boundary conditions. The bifurcation analysis aims to identify a non-trivial perturbed solution $\boldsymbol{v}$, i.e., the difference between the inhomogeneous and homogeneous velocity fields.

Undrained solid-fluid instability: The general expression for perturbed velocity field associated with solid-fluid (SF) instability

$$\begin{aligned} v_1 &= V_1 \sin(\gamma_1 x_1 + \theta_1)\cos(\beta_2 x_2 + \theta_2) f(t) \\ v_2 &= V_2 \cos(\gamma_1 x_1 + \theta_1)\sin(\beta_2 x_2 + \theta_2) f(t) \\ \dot{p} &= P \cos(\beta_1 x_1 + \theta_1)\cos(\beta_2 x_2 + \theta_2) f(t), \end{aligned} \tag{7}$$

where V_1, V_2, P are the are arbitrary modal amplitudes, $f(t)$) is an unknown function of time. The coefficients β_1, β_2, γ_1, θ_1, θ_2 are such that they should satisfy the respective boundary conditions. Eq. 7 along with Eq. 5 and 6 leads to the condition for SF instability. For an infinite growth of SF instability under flexible lateral boundary following condition should get satisfied

$$\bar{G} = (d_4 + d_7)\gamma_1^2\beta_2^2 - \beta_2^2(d_1\gamma_1^2 + d_3\beta_2^2) + \frac{l_2}{l_1}\frac{l_3}{l_4}\left\{(d_4 + d_8)\gamma_1\beta_1\beta_2^2 - (d_5\gamma_1^2 + d_2\beta_2^2)\gamma_1\beta_1\right\} = 0, \tag{8}$$

where $l_1 = \sin(\gamma_1 x_1 + \theta_1), l_2 = \cos(\gamma_1 x_1 + \theta_1), l_3 = \sin(\beta_1 x_1 + \theta_1), l_4 = \cos(\beta_1 x_1 + \theta_1),$

$$d_1 = C_{1111} - \sigma_{11}, d_2 = C_{2222} - \sigma_{22}, d_7 = C_{1122}, d_8 = C_{2211}, d_3 = C_{1212} - (\sigma_{11} - \sigma_{22})/2,$$
$$d_4 = C_{1212} - (\sigma_{11} + \sigma_{22})/2, d_5 = C_{1212} + (\sigma_{11} - \sigma_{22})/2, d_6 = C_{1212} + (\sigma_{11} + \sigma_{22})/2.$$

This equation is defined within the domain $-L_1 \le x_1 \le L_1$ except at $x_1 = 0$. However, it can be evaluated near $x_1 = 0$ by $\bar{G}_{0+} = \lim_{x_1 \to 0} \bar{G}$, which satisfies Eq. 8 first compared to other values of x_1. For a fundamental mode it is given by the following

$$\bar{G}_{0+} = \lim_{x_1 \to 0} \bar{G} = (2d_4 + d_7 + d_8 - d_1 - d_2)\gamma_1^2\beta_2^2 - d_3\beta_2^4 - d_5\gamma_1^4. \tag{9}$$

The perturbed velocity field and the condition of emergence for SF instability under rigid boundary case can be retrieved from Eq. 7 and 8 when $\gamma_1 = \beta_1$ is enforced (Mukherjee et al., 2016a) along with the boundary condition of Figure 1(b).

Drained diffused mode: The drained diffused modes can be presented by the following expression

$$v_1(x_1,x_2) = V_1(x_1)\cos(\beta x_2 + \theta_2)$$
$$v_2(x_1,x_2) = V_2(x_1)\sin(\beta x_2 + \theta_2) \quad (10)$$

The coefficients β and θ_2 are selected such that the velocity fields should satisfy the boundary condition of Figure 1(c). A general form of velocity solution can be assumed as $V_1(x_1) = Ae^{i\alpha x_1}$ and $V_2(x_1) = Be^{i\alpha x_1}$, which when substituted in the equilibrium equation leads to the following characteristic equation

$$a_1 Z^4 + b_1 Z^2 + c_1 = 0, \quad (11)$$

where $a_1 = d_1 d_5, b_1 = d_1 d_2 + d_3 d_5 - (d_4 + d_7)(d_4 + d_8), c_1 = d_2 d_3, Z = \alpha/\beta.$

Depending on magnitudes of a_1, b_1 and c_1, Eq. 11 has four different types of solution in Z, elliptic imaginary, elliptic complex, parabolic and hyperbolic. The drained diffused modes are examined here in elliptic complex regime for flexible lateral boundaries; whereas, these modes can only be obtained in hyperbolic regime for rigid lateral boundary case due to the boundary constraint of Figure 1(d). However, in hyperbolic regime the localized modes remain in competition with such diffused modes. The details of the drained diffused velocity modes along with their emergence equations can be found in Bardet (1991).

Localization mode: Strain can bifurcate into localized modes in form of shear band and the velocity continuity for cases requires (Rice 1976), $[\![v_{i,j}]\!] = g_i n_j$, where $[\![.]\!]$ denotes the jump in the field variable within and outside the band, $\boldsymbol{g}$ is an arbitrary vector and $\boldsymbol{n}$ is the normal to the band. The velocity continuity along with stress equilibrium across the band leads to the same characteristics equation as in Eq. 11. Two unique real solutions for $\boldsymbol{n}$ are obtained on elliptic/hyperbolic boundary. This also corresponds to the loss of positive definiteness of the acoustic tensor. The shear band angle (θ_s) from lateral direction (i.e., clockwise from x_1-axis) can be calculated by substituting $n_1 = \sin(\theta_s)$, $n_2 = \cos(\theta_s)$. In case of localization analysis under undrained condition, a locally drained condition has been assumed near the localization zone. The analysis procedure is same as the drained case; however, the coefficients of Eq. 11 are now calculated based on the effective stress parameters. The localization modes remain independent of the type of lateral boundary condition imposed during the bifurcation analysis.

INSTABILITY PREDICTION

Undrained and drained simulations are carried out on medium dense Hostun RF sand with initial void ratio $e_0 = 0.7 - 0.75$ and initial effective confining pressure varying from 50-400 kPa. The homogeneous stress-strain field is obtained by integrating the elasto-plastic constitutive equations numerically. An objective algorithm based on the notion of rotated configuration has been used in conjunction with the explicit return mapping (Dodds and Healy 2001). The homogeneous stress-strain field is used to identify the possible onset of various instability modes; however, the actual post-instability behavior has not been explored in this study.

Undrained instability: The undrained stress-path at two initial effective confining pressures have been presented in Figure 2(a) and 2(b) for varying e_0. At lower confining pressure (100

kPa), initially contractive response has been noticed for cases with $e_0 = 0.7 - 0.75$ followed by a distinct phase change. This is a typical behavior of medium dense sand. The response becomes more contractive with increase in the initial confinement (400 kPa), which can also be noticed from 2(c) and 2(d), i.e., the stress paths of medium dense sands at varying confinement. The onset of localization and SF instability under rigid and flexible condition has been marked in Figure 2. In case of rigid lateral boundaries, SF instability emerges first, i.e., just before the peak stress and then followed by the localized mode; whereas, for flexible case localization precedes the SF modes. In all of these cases, both SF instability and localization get delayed with increase in the confinement. For simulation with $e_0 = 0.7$ under rigid boundary, the nature of first instability mode changes from SF to localization with increase in the confinement; however, only localization type of instability has been captured for $e_0 = 0.7$ under flexible boundary condition.

Drained instability: The drained stress-strain response, volumetric behaviour and predicted instability modes are presented in Figure 3 for medium dense sand $e_0 = 0.75$. A monotonically increasing shear stress response has been noticed for the confinement range 50-300 kPa with initially contractive and then followed by a dilative volumetric response. The drained diffused antisymmetric modes are captured only for cases with flexible lateral boundary condition. Furthermore, these modes emerge at higher confining pressure (≥ 200 kPa) for slender specimens with aspect ratio $L_2/L_1 = 3$; however, once activated it nearly remains independent of the level of confinement. On the contrary, localization is noticed to emerge over the complete confinement range under consideration and its onset is delayed with increase in the initial confining pressure. The localization onset also gets retarded with reduction in the magnitude of shear modulus as depicted in Figure 4(a) for $\mu = G_0/6$. In this case, the diffused antisymmetric modes start to emerge even at lower confinements for specimen with $L_2/L_1 = 3$. In addition, such modes are also encountered now for specimen with lower aspect ratio, i.e., $L_2/L_1 = 2$ at higher confinement. If the shear modulus is reduced further ($\mu = G_0/8$), the symmetric diffused modes start to appear in bulky specimens ($L_2/L_1 = 1$) of denser sand with $e_0 = 0.7$ at very high confinement, e.g., 600 kPa (Figure 4b). The influence of confining pressure on drained and undrained localization onset & shear band angle have been presented in Figure 5. As mentioned earlier, onsets for both types of localization get delayed with increasing confinement. Unlike drained case, undrained localization angle increases with increase in the confinement level. For undrained shearing, the increasing shear stress ratio and dilation angle at the onset of localization might have attributed to such increase in the shear band angle (Mukherjee et al. 2016a).

CONCLUSION

Plane strain bifurcation analysis was carried out to explore instability behavior of medium dense sand under both drained and undrained biaxial shearing. Large deformation framework was employed along with a 3D material model to capture various instability modes under rigid and flexible lateral boundaries. In case of undrained test, Solid-Fluid instability emerges first under rigid boundary condition; whereas, such modes get significantly delayed under flexible boundaries and can even be preceded by localization. Drained diffused modes are captured only when analysed with flexible lateral boundaries. Drained antisymmetric diffused modes are more prone to emerge in slender samples at higher confinement; whereas, symmetric diffused modes are found for bulky samples at very high confinement. Both drained and undrained localization

get delayed with increase in the level of confinement. A reduction in the magnitude of shear modulus retards the onset of localized instability and favors the initiation of diffused instability modes.

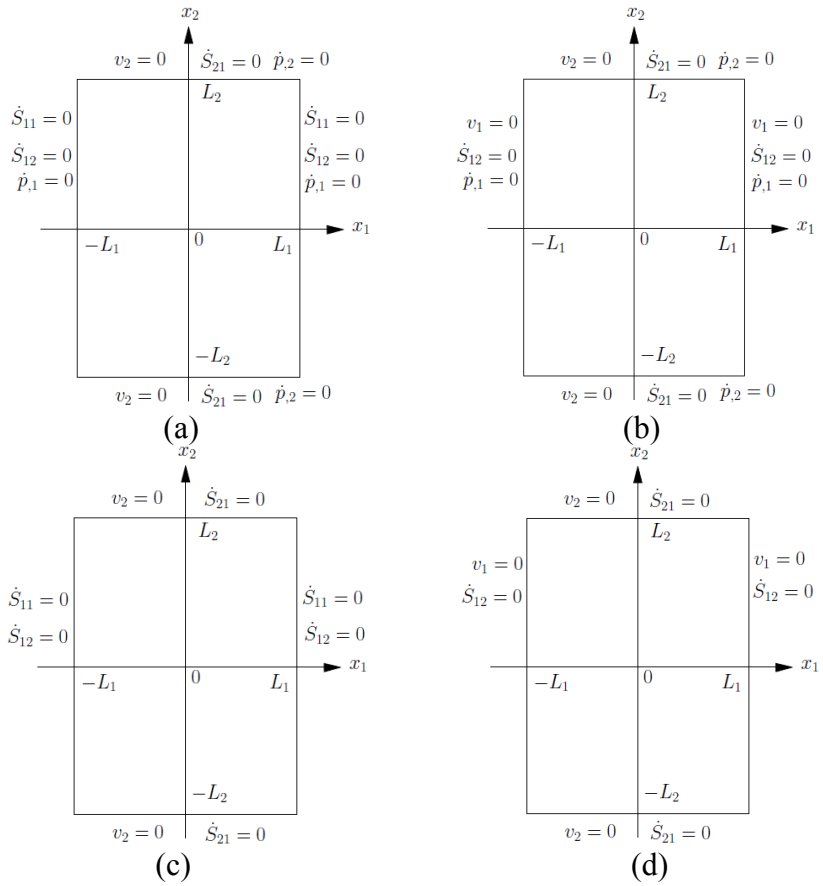

Figure 1. Boundary conditions for plane strain bifurcation with (a,c) flexible and (b,d) rigid boundary condition under undrained and drained loading, respectively ($\boldsymbol{v}$, $\boldsymbol{S}$, p denotes the velocity field, nominal stress tensor and pore pressure, respectively).

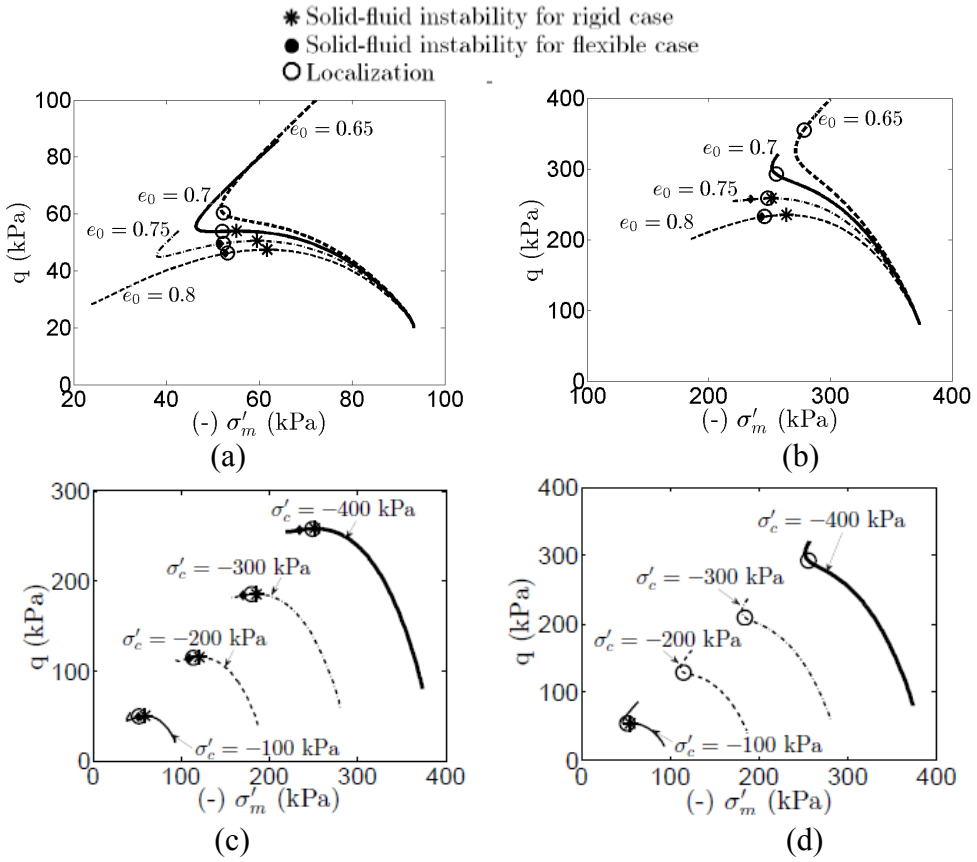

Figure 2. Stress-paths for (a) $\sigma_c^{'}$ = -100 kPa and (b) $\sigma_c^{'}$ = -400 kPa for varying e_0 & (c) e_0 =0.75 and (d) e_0 =0.7 for varying initial effective confinement ($\sigma_c^{'}$). In the figure q, $\sigma_m^{'}$, ε_q are the shear stress, effective mean pressure, and shear strain, respectively.

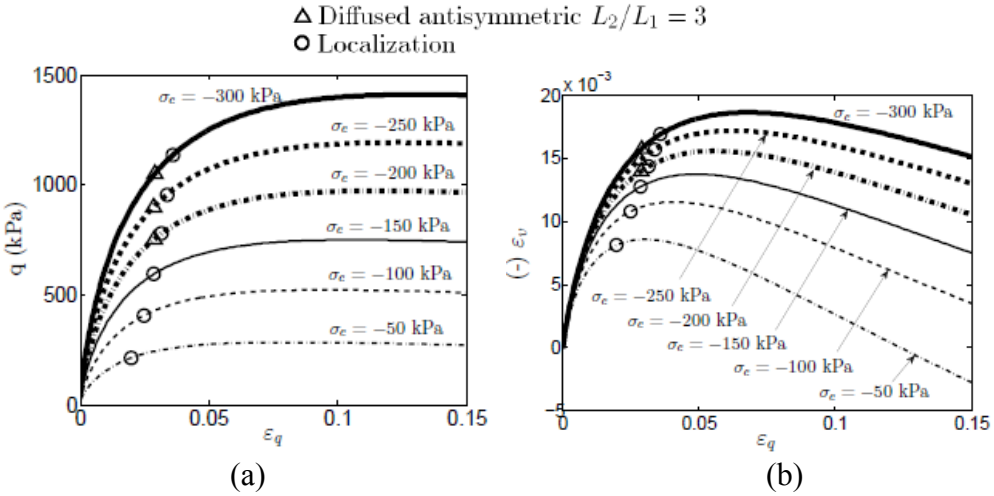

Figure 3. (a) Stress-strain and (b) volumetric response of medium sand (e_0 =0.75) under drained biaxial loading with varying initial confinement ($\mu = G_0/3$).

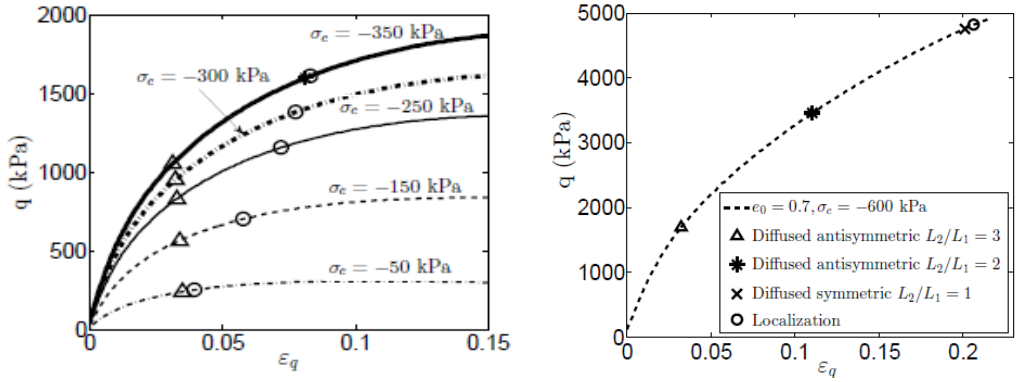

(a) (b)

Figure 4. Stress-strain response of medium sand under drained biaxial loading for (a) e_0 =0.75 ($\mu = G_0/6$) and (b) e_0 =0.7 ($\mu = G_0/8$).

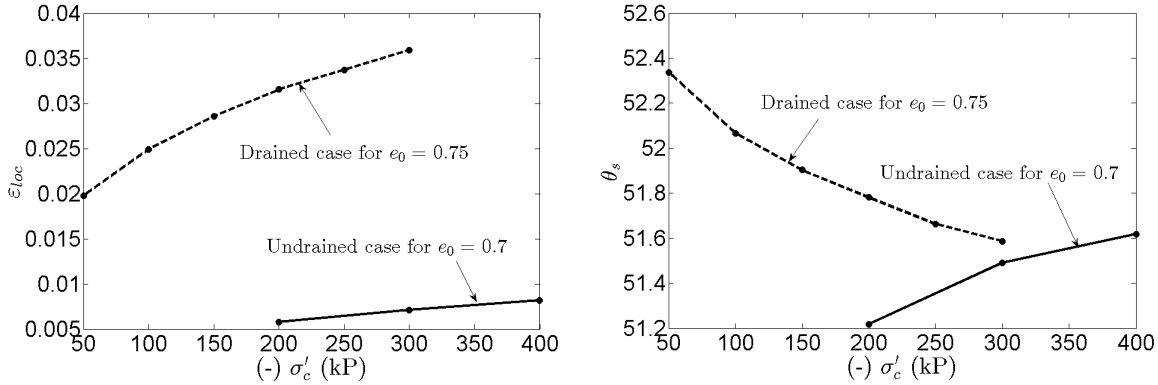

(a) (b)

Figure 5. Variation of (a) onset shear strain for localization ε_{loc} and (b) shear band angle θ_S for both drained and undrained case (considering rigid lateral boundary).

REFERENCES

Bardet, J. P. (1991). "Analytical solutions for the plane-strain bifurcation of compressible solids." J. App. Mech., 58, 651-657.

Bardet, J. P., Shiv, A. (1995). "Plane-strain instability of saturated porous media." J. Eng. Mech., 121, 717-724.

Desrues, J., and Hammad, W. (1989). "Shear banding dependency on mean stress level in sand." 2nd Int. Workshop on Numerical Methods for Localization and Bifurcation of Granular Bodies, Gdansk-Karlsruhe, E. Dembicki, G. Gudehus, and Z. Sikora, eds., Technical Univ. of Gdansk, Gdansk, Poland, 57–67.

Desrues, J., Lanier, J., and Stutz, P. (1985). "Localization of the deformation in tests on sand sample." Eng. Fract. Mech., 21(4), 909–921.

Finno, R. J., Harris, W. W., Mooney, M. A., Viggiani, G. (1997). Shear bands in plane strain compression of loose sand." *Geotechnique*, 47(1), 149-165.

Gajo, A., Bigoni, D., Wood, D. M., 2004. Multiple shear band development and related instabilities in granular materials. J. Mech. Phys. Solids, 52, 2683-2724.

Han, C., Drescher, A. (1993). "Shear bands in biaxial tests on dry coarse sand." Soils Found., 33(1), 118-132.

Han, C., Vardoulakis, I. (1991). "Plane strain compression experiments on water saturated fine grained sand." *Geotechnique*, 41(1), 49-78.

Hardin, B. O., Black, W. L. (1966). "Sand stiffness under various triaxial stresses." J. Soil Mech. Found. Eng. Div., 91(SM2), 353-369.

Hill, R., Hutchinson, J. W. (1975). "Bifurcation phenomena in the plane tension test." J. Mech. Phys. Solids, 23, 239-264.

Mukherjee, M., Gupta, A., Prashant, A. (2016a). "Instability analysis of sand under undrained biaxial loading with rigid and flexible boundary", Int. J. Geomech., 10.1061/(ASCE)GM.1943-5622.0000690.

Mukherjee, M., Gupta, A., Prashant, A. (2016b). "Drained instability analysis of sand under biaxial loading using a 3D material model", Comp. Geotech., 10.1016/j.compgeo.2016.05.023.

Needleman, A. (1979). "Non-normality and bifurcation in plane strain tension and compression." J. Mech. Phys. Solids, 27, 231-254.

Rice, J. R. (1976). "The localization of plastic deformation." Proc., 14th Int. Congress on Theoretical and Applied Mechanics, Vol. 1, North-Holland Publishing, Amsterdam, Netherlands, 207–220.

Vardoulakis, I. (1981). "Bifurcation analysis of the plane rectilinear deformation on dry sand samples." Int. J. Solids Struct., 17(11), 1085-1101.

Vardoulakis, I., 1985. Stability and bifurcation of undrained, plane rectilinear deformations on water-saturated granular soils. Int. J. Numer. Anal. Methods Geomech., 9, 399-414.

Wood, D. M. (2004). Geotechnical Modeling. CRC Press, Taylor and Francis group.